

An alternative extended linear system for boundary value problems on locally perturbed geometries

Y. Zhang and A. Gillman

Abstract

This manuscript presents a new extended linear system for integral equation based techniques for solving boundary value problems on locally perturbed geometries. The new extended linear system is similar to a previously presented technique for which the authors have constructed a fast direct solver. The key features of the work presented in this paper are that the fast direct solver is more efficient for the new extended linear system and that problems involving specialized quadrature for weakly singular kernels can be easily handled. Numerical results illustrate the improved performance of the fast direct solver for the new extended system when compared to the fast direct solver for the original extended system.

1 Introduction

This manuscript presents an integral equation based solution technique for elliptic boundary value problems on locally-perturbed geometries. Such problems arise in applications such as optimal shape design. In each iteration or optimization cycle, the changes to the object shape often stay local to certain parts of the object. The proposed approach formulates an extended linear system that allows for the boundary value problem on the new geometry to be expressed in terms of a linear system on the original geometry plus a correction to account for the local perturbation. This idea was first proposed in [4] and a fast direct solver was constructed for the resulting formulation in [9]. Unfortunately, the fast direct solver for the original extended system required inverting a matrix the size of the number of points removed from the original geometry which is expensive if the removed portion is large. Another difficulty of the original extended system is that care is required when the technique is applied to systems discretized using quadrature for weakly singular kernels. The extended linear system proposed in this manuscript overcomes these two difficulties. Additionally, a fast direct solver for the new extended system can be constructed from the tools presented in [9] but is more efficient than the original fast direct solver.

This manuscript briefly reviews a boundary integral formulation for a Laplace problem with Dirichlet boundary data and the linear system that results from the discretization in Section 2. Next, the original extended system and the new extended system are presented in Section 3. Finally numerical results illustrate the efficiency of the fast direct solver for the new extended system in Section 4.

2 Boundary integral formulation

Consider the interior Laplace problem with Dirichlet boundary condition

$$\begin{aligned} -\Delta u(\mathbf{x}) &= 0 & \text{for } \mathbf{x} \in \Omega, \\ u(\mathbf{x}) &= g(\mathbf{x}) & \text{for } \mathbf{x} \in \Gamma \end{aligned} \tag{1}$$

where Ω denotes the interior of the geometry, and Γ denotes the boundary of Ω , as illustrated in Figure 1(a). Let $G(\mathbf{x}, \mathbf{y}) = -\frac{1}{2\pi} \log |\mathbf{x} - \mathbf{y}|$ denote the Green's function for the Laplace operator and $D(\mathbf{x}, \mathbf{y}) =$

$\partial_{n(\mathbf{y})}G(\mathbf{x}, \mathbf{y})$ denote the double layer kernel where $n(\mathbf{x})$ denotes the outward facing normal vector at the point $\mathbf{x} \in \Gamma$. The solution to (1) can be expressed as

$$u(\mathbf{x}) = \int_{\Gamma} D(\mathbf{x}, \mathbf{y})\sigma(\mathbf{y})ds(\mathbf{y}) \quad \text{for } \mathbf{x} \in \Omega, \quad (2)$$

where $\sigma(\mathbf{x})$ is some unknown density defined only on the boundary Γ . Enforcing that $u(\mathbf{x})$ satisfies the boundary condition results in the following integral equation for $\sigma(\mathbf{x})$;

$$-\frac{1}{2}\sigma(\mathbf{x}) + \int_{\Gamma} D(\mathbf{x}, \mathbf{y})\sigma(\mathbf{y})ds(\mathbf{y}) = g(\mathbf{x}). \quad (3)$$

Upon discretization via a Nyström or boundary element method, one is left with solving a dense linear system

$$\mathbf{A}\boldsymbol{\sigma} = \mathbf{g}, \quad (4)$$

where \mathbf{A} is the discretized boundary integral operator and $\boldsymbol{\sigma}$ is the vector approximating σ at the discretization points.

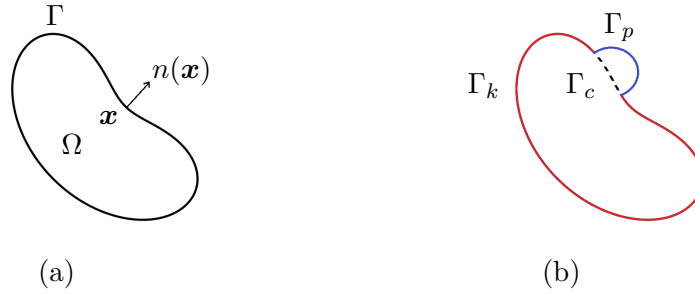


Figure 1: (a) A sample geometry Ω with boundary Γ and outward facing normal vector $n(\mathbf{x})$ at the point $\mathbf{x} \in \Gamma$. (b) A sample locally perturbed geometry where the original boundary is $\Gamma_o = \Gamma_k \cup \Gamma_c$, the portion of the boundary being removed is Γ_c , the portion of the original boundary remaining is Γ_k and the newly added boundary is Γ_p .

3 Extended linear systems

Consider a boundary value problem on a geometry with a local perturbation as illustrated in Figure 1(b). Let Γ_o denote the boundary of the original geometry, Γ_k denote the portion of the boundary that is not changing and Γ_c denote the portion that is cut or removed. So $\Gamma_o = \Gamma_c \cup \Gamma_k$. Let Γ_p denote the new portion of the boundary. Then the new geometry has a boundary Γ_n defined by $\Gamma_n = \Gamma_k \cup \Gamma_p$.

The discretized linear systems can be partitioned according to this notation. In other words, the original system can be expressed as

$$\mathbf{A}_{oo}\boldsymbol{\tau}_o = \begin{bmatrix} \mathbf{A}_{kk} & \mathbf{A}_{kc} \\ \mathbf{A}_{ck} & \mathbf{A}_{cc} \end{bmatrix} \begin{pmatrix} \boldsymbol{\tau}_k \\ \boldsymbol{\tau}_c \end{pmatrix} = \begin{pmatrix} \mathbf{g}_k \\ \mathbf{g}_c \end{pmatrix} = \mathbf{g}_o, \quad (5)$$

and the linear system for the perturbed geometry can be expressed as

$$\mathbf{A}_{nn}\boldsymbol{\sigma}_n = \begin{bmatrix} \mathbf{A}_{kk} & \mathbf{A}_{kp} \\ \mathbf{A}_{pk} & \mathbf{A}_{pp} \end{bmatrix} \begin{pmatrix} \boldsymbol{\sigma}_k \\ \boldsymbol{\sigma}_p \end{pmatrix} = \begin{pmatrix} \mathbf{g}_k \\ \mathbf{g}_p \end{pmatrix} = \mathbf{g}_n \quad (6)$$

where $\boldsymbol{\tau}_k$ and $\boldsymbol{\sigma}_k$ denote the vector whose entries are the approximate solution at the discretization points on Γ_k , $\boldsymbol{\tau}_c$ denotes the vector whose entries are the approximate solution at the discretization points on Γ_c , etc. Likewise \mathbf{A}_{kk} is the submatrix of the discretized integral equation corresponding to the interaction of Γ_k with itself, \mathbf{A}_{kc} is the submatrix of the discretized integral equation corresponding to the interaction of Γ_k with Γ_c , etc.

3.1 Original extended linear system

The discretized problem on Γ_n can be expressed as an extended linear system [4] by

$$\left(\underbrace{\begin{bmatrix} \mathbf{A}_{oo} & \mathbf{0} \\ \mathbf{0} & \mathbf{A}_{pp} \end{bmatrix}}_{\mathbf{A}} + \underbrace{\begin{bmatrix} 0 & \begin{pmatrix} -\mathbf{A}_{kc} \\ -\mathbf{B}_{cc} \end{pmatrix} & \mathbf{A}_{op} \\ \mathbf{A}_{pk} & 0 & 0 \end{bmatrix}}_{\mathbf{Q}_{\text{orig}}} \right) \underbrace{\begin{pmatrix} \sigma_k \\ \sigma_c \\ \sigma_p \end{pmatrix}}_{\sigma_{\text{ext}}} = \underbrace{\begin{pmatrix} \mathbf{g}_k \\ \mathbf{0} \\ \mathbf{g}_p \end{pmatrix}}_{\mathbf{g}_{\text{ext}}} \quad (7)$$

where \mathbf{A}_{kc} denotes the submatrix of \mathbf{A}_{oo} corresponding to the interaction between Γ_k and Γ_c , \mathbf{A}_{op} denotes the discretization of the double layer integral operator on Γ_p evaluated on Γ_o , \mathbf{A}_{pk} denotes the discretization of the double layer integral operator on Γ_k evaluated on Γ_p , and \mathbf{B}_{cc} denotes the sub-matrix of \mathbf{A}_{oo} corresponding to the interaction of Γ_c with itself but the diagonal entries are set to zero. The matrix \mathbf{Q}_{orig} is called the *update matrix*. The extended system (7) is obtained by subtracting the contributions from Γ_c in \mathbf{A}_{oo} and adding the contributions from Γ_p . Upon solving (7), only σ_k and σ_p are used to evaluate the solution inside of Γ_n . Effectively σ_c is a dummy vector. Details of the derivation of (7) are provided in [4, 9].

3.2 New extended linear system

The new extended linear system exploits the fact that the contribution from Γ_c is not used to find the solution inside of Γ_n . Specifically, we introduce the vector σ_c^{dum} fully knowing a priori that it will contain useless information. Then solving (6) is equivalent to solving the following

$$\begin{bmatrix} \mathbf{A}_{kk} & \mathbf{0} & \mathbf{A}_{kp} \\ \mathbf{A}_{ck} & \mathbf{A}_{cc} & \mathbf{0} \\ \mathbf{A}_{pk} & \mathbf{0} & \mathbf{A}_{pp} \end{bmatrix} \begin{pmatrix} \sigma_k \\ \sigma_c^{\text{dum}} \\ \sigma_p \end{pmatrix} = \begin{pmatrix} \mathbf{g}_k \\ \mathbf{0} \\ \mathbf{g}_p \end{pmatrix}. \quad (8)$$

The expanded form of (8) is

$$\left(\underbrace{\begin{bmatrix} \mathbf{A}_{oo} & \mathbf{0} \\ \mathbf{0} & \mathbf{A}_{pp} \end{bmatrix}}_{\mathbf{A}} + \underbrace{\begin{bmatrix} \mathbf{0} & -\mathbf{A}_{kc} & \mathbf{A}_{kp} \\ \mathbf{0} & \mathbf{0} & \mathbf{0} \\ \mathbf{A}_{pk} & \mathbf{0} & \mathbf{0} \end{bmatrix}}_{\mathbf{Q}_{\text{new}}} \right) \underbrace{\begin{pmatrix} \sigma_k \\ \sigma_c^{\text{dum}} \\ \sigma_p \end{pmatrix}}_{\sigma_{\text{ext}}} = \underbrace{\begin{pmatrix} \mathbf{g}_k \\ \mathbf{0} \\ \mathbf{g}_p \end{pmatrix}}_{\mathbf{g}_{\text{ext}}}. \quad (9)$$

Here \mathbf{Q}_{new} is the new update matrix. Notice that \mathbf{Q}_{new} has a zero row. As compared to the original formulation (7), the new formulation has two advantages: first, the update matrix no longer contains the full-rank block \mathbf{B}_{cc} ; second the new formulation does not require evaluating \mathbf{A}_{cp} . We postpone the discussion for the first advantage to Section 3.3. For the problems considered in this paper, N_c and N_p are relatively small compared to N_k , thus evaluating and compressing \mathbf{A}_{cp} is not expensive if the kernel is analytic. However, for problems where the perturbation corresponds to local refinement of the same geometry, the collection of discretization points removed I_c and those added I_p correspond to different discretizations of the same boundary segment $\Gamma_c = \Gamma_p$. This means that the evaluation of \mathbf{A}_{cp} requires additional care when the kernel is weakly singular. By not including this matrix in the new formulation, the problem of handling weakly singular kernels (such as when using a combined field integral representation for Helmholtz problems) is removed.

3.3 A fast direct solver

When constructing the fast direct solver for the locally perturbed boundary value problem, there are advantages to writing the system in the form of (7) and (9). Since the matrix \mathbf{A}_{oo} is the system resulting

from the discretization of the integral equation on the original geometry, we assume that a fast direct solver has already been computed for \mathbf{A}_{oo} . Any fast direct solver such as *Hierarchically Block Separable (HBS)* [3], *Hierarchically Semi-Separable (HSS)* [8, 1], *Hierarchical Interpolative Factorization (HIF)* [6] and \mathcal{H} and \mathcal{H}^2 -matrix methods [5] can be used. Additionally, the update matrices \mathbf{Q}_{orig} and \mathbf{Q}_{new} are low rank. This allows for the inverse of the extended systems to be applied rapidly via a Sherman-Morrison-Woodbury formula

$$\boldsymbol{\sigma}_{\text{ext}} = \left(\tilde{\mathbf{A}} + \mathbf{Q}\right)^{-1} \mathbf{g}_{\text{ext}} \approx \left(\tilde{\mathbf{A}} + \mathbf{LR}\right)^{-1} \mathbf{g}_{\text{ext}} \approx \tilde{\mathbf{A}}^{-1} \mathbf{g}_{\text{ext}} - \tilde{\mathbf{A}}^{-1} \mathbf{L} \left(\mathbf{I} + \mathbf{R}\tilde{\mathbf{A}}^{-1} \mathbf{L}\right)^{-1} \mathbf{R}\tilde{\mathbf{A}}^{-1} \mathbf{g}_{\text{ext}}, \quad (10)$$

where \mathbf{I} is an identity matrix, and \mathbf{LR} denotes the low rank factorization of the update matrix \mathbf{Q} .

The low rank property of the update matrices \mathbf{Q}_{orig} and \mathbf{Q}_{new} can be observed by noting that the matrices \mathbf{A}_{kc} , \mathbf{A}_{kp} , \mathbf{A}_{pk} and \mathbf{A}_{op} are low rank. The only full rank matrix in the update matrices is \mathbf{B}_{cc} . Let k_{op} , k_{kc} , k_{pk} , and k_{kp} be the observed numerical ranks for matrix \mathbf{A}_{op} , \mathbf{A}_{kc} , \mathbf{A}_{kp} , \mathbf{A}_{kp} respectively. Then the low-rank approximation for \mathbf{Q}_{orig} has total rank $k_{\text{orig}} = k_{op} + k_{kc} + k_{pk} + N_c$. Since \mathbf{Q}_{new} does not contain the \mathbf{B}_{cc} matrix, its rank is $k_{\text{new}} = k_{kc} + k_{pk} + k_{kp}$, which is smaller than \mathbf{Q}_{orig} . Thus the Sherman-Morrison-Woodbury formula can be applied more rapidly with the new formulation. The details for efficiently creating the low rank factorizations can be found in [9].

4 Numerical experiments

This section illustrates the performance of the fast direct solver for the proposed extended linear system for a collection of problems. The integral equations are discretized via the Nyström method with a 16-point composite Gaussian quadrature. For all problems, the original geometry is discretized with enough points in order for the boundary value problem to be solved to 10 digits of accuracy. The HBS direct solver [3] was used in the examples in this section. For all tests, the tolerance for HBS compression and low-rank approximation is set to $\epsilon = 10^{-10}$.

Roughly speaking the cost of building fast direct solvers is split into two parts: precomputation and solve. The time for precomputation is the time for constructing all the parts of the fast direct solver. For the extended systems, this includes constructing the low rank factorizations of the update matrices \mathbf{Q}_{orig} or \mathbf{Q}_{new} and inverting the small matrix in the Sherman-Morrison-Woodbury formula (10). For the HBS solver, the precomputation includes creating a compressed approximation of the discretized system on the new geometry and inverting that approximation. The solve time is the time for applying the resulting solver to one vector (or right-hand-side). For the extended systems, this is the time for applying the Sherman-Morrison-Woodbury formula (10). For the HBS solver, it is the time for applying the approximate inverse.

To illustrate the efficiency of the proposed technique, we compare the performance of the new solution technique with the fast solver developed for the original extended system and building an HBS solver from scratch for the new geometry. We report the following:

- N_o : the number of discretization points on the original geometry;
- N_c : the number of discretization points cut from the original geometry;
- N_k : the number of discretization points remained the same on the original and new geometry, $N_k = N_o - N_c$;
- N_p : the number of discretization points added;
- k_{op} , k_{kc} , k_{pk} , and k_{kp} : the observed numerical ranks for matrix \mathbf{A}_{op} , \mathbf{A}_{kc} , \mathbf{A}_{kp} , and \mathbf{A}_{kp} respectively after compression;
- k_{new} and k_{orig} : the observed numerical ranks for \mathbf{Q}_{new} and \mathbf{Q}_{orig} respectively, $\mathbf{Q}_{\text{new}} = k_{kc} + k_{kp} + k_{pk}$ and $\mathbf{Q}_{\text{orig}} = k_{op} + k_{kc} + k_{pk} + N_c$;

- $T_{\text{new},p}$: the time in seconds for the precomputation of the proposed solver;
- $T_{\text{orig},p}$: the time in seconds for the precomputation of the fast solver based on the original extended system formulation in [9];
- $T_{\text{hbs},p}$: the time in seconds for the precomputation of HBS from scratch for the new geometry;
- $r_p = \frac{T_{\text{hbs},p}}{T_{\text{new},p}}$;
- $T_{\text{new},s}$: the time in seconds for applying the proposed solver to one right-hand-side;
- $T_{\text{orig},s}$: the time in seconds for applying the original solver in [9] to one right-hand-side;
- $T_{\text{hbs},s}$: the time in seconds for applying the HBS inverse to one right-hand-side;
- $r_s = \frac{T_{\text{hbs},s}}{T_{\text{new},s}}$.

The ratios r_p and r_s are measures for the speed-up (or slow-down) by using the proposed solver versus building a new fast direct solver from scratch for the new geometry. If r_p is greater than 1, the precomputation of the proposed solver is faster than building a fast direct solver from scratch. If r_p is less than 1, the precomputation of the proposed solver is slower than building a fast direct solver from scratch, etc.

All experiments were run on a dual 2.3 GHz Intel Xeon Processor E5-2695 v3 desktop workstation with 256 GB of RAM. The code is implemented in MATLAB, apart from the randomized linear algebra utilized in creating low rank factorization rapidly which is implemented in Fortran.

4.1 A local change in the geometry

Consider the Laplace boundary value problem (1) on the geometry illustrated in Figure 2. The corners are smoothed via the scheme in [2]. A detailed description of this geometry is given in [9]. The Dirichlet data on the boundary equals to the potential due to a collection of 10 charges with location and charge value $\{(\mathbf{s}_j, q_j)\}_{j=1}^{10}$ placed on the exterior of domain Ω ,

$$g(\mathbf{x}) = \sum_{j=1}^{10} q_j G(\mathbf{x}, \mathbf{s}_j),$$

where $G(\mathbf{x}, \mathbf{y})$ denotes the Green's function for Laplace equation.

In the first experiment, the number of points cut remains fixed, $N_c = 16$, while the number of discretization points on Γ_k grows. In Figure 2, this corresponds to the nose height d decreasing as N_k grows. The attached nose Γ_p is discretized with $N_p \in [832, 896]$ number of quadrature points. The timing results are reported in Table 1. All three solution techniques are linear with respect to N_o and the precomputation time for the new solution technique is about the same as the original extended system solver. It is roughly 3.5 times faster than building a new direct solver from scratch for the new geometry. The cost of applying the proposed solver is almost as fast as applying the HBS approximate inverse. To better understand the new extended system formulation's performance as compared to the original formulation in [9], Table 2 reports the numerical ranks for the subblocks in \mathbf{Q}_{orig} and \mathbf{Q}_{new} . The total rank of \mathbf{Q}_{new} is observed to be smaller than that for \mathbf{Q}_{orig} by about 20, which is not a very significant reduction. This explains the timing results in Table 1, where the timings in column $T_{\text{orig},p}$ is slightly larger than those in column $T_{\text{new},p}$ for large tests.

In the next example, N_c grows by the same factor as N_k . The nose height d in Figure 2 remains fixed, and the fixed nose is discretized with $N_p = 896$ points. Table 3 reports on the performance of all three solvers for this geometry. The proposed solution technique is the fastest for the precomputation step. It is much faster than the solver based on the original extended system formulation, especially for the case where N_c is large. The ranks of the compressed matrices are reported in Table 4. Since N_c grows at

the same rate as N_k while the problem size increases, k_{orig} becomes very large and the dense inversion of $(\mathbf{I} + \mathbf{R}\tilde{\mathbf{A}}^{-1}\mathbf{L})$ dominates the cost of evaluating the solution of the original extended system. This is in contrast to the new formulation where k_{new} does not depend on N_c and thus the new solver is much faster than both the original solver in [9] and HBS built from scratch for precomputation. A factor of roughly 2.9 speed up in the precomputation is observed as compared to an HBS solver built from scratch. Again applying the proposed solver is slightly slower than applying the HBS approximate inverse.

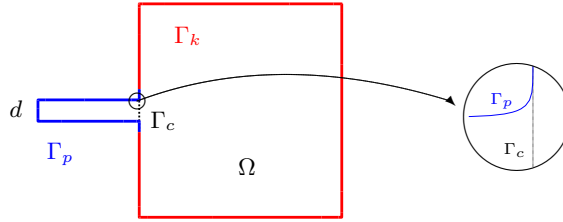


Figure 2: The square with nose geometry. A nose of height d is smoothly attached to the a square.

N_o	$T_{\text{orig},p}$	$T_{\text{new},p}$	$T_{\text{hbs},p}$	r_p	$T_{\text{orig},s}$	$T_{\text{new},s}$	$T_{\text{hbs},s}$	r_s
9232	3.69e-01	4.83e-01	1.57e+00	3.25	1.99e-02	1.12e-02	1.32e-02	1.18
18448	5.60e-01	6.50e-01	2.38e+00	3.66	2.76e-02	1.74e-02	1.46e-02	0.84
36880	1.11e+00	1.11e+00	3.79e+00	3.42	5.49e-02	4.00e-02	3.33e-02	0.83
73744	2.25e+00	1.84e+00	6.38e+00	3.47	9.79e-02	8.06e-02	7.04e-02	0.87
147472	3.87e+00	3.56e+00	1.18e+01	3.33	1.95e-01	1.71e-01	1.52e-01	0.89

Table 1: Times for applying the solution technique to (1) on the square with thinning nose geometry.

N_o	N_c	k_{op}	k_{kc}	k_{pk}	k_{kp}	k_{orig}	k_{new}
9232	16	63	9	54	60	142	123
18448	16	64	10	58	58	148	126
36880	16	66	10	57	61	149	128
73744	16	68	10	59	60	153	129
147472	16	69	10	61	61	156	132

Table 2: Observed numerical ranks for compressed matrices in the original and new extended system formulations for the square with thinning nose geometry.

4.2 A Laplace problem with a locally refined discretization

Next we consider applying the proposed solution technique to the Laplace boundary value problem (1) where the local perturbation is a refinement in a portion of the geometry. Figure 3(a) illustrates the geometry under consideration. It is given by the following parameterization:

$$\mathbf{x}(t) = \begin{pmatrix} r(t) \cos(t) \\ r(t) \sin(t) \end{pmatrix}, \text{ with } r(t) = 1 + 0.3 \sin(30t) \text{ for } t \in [0, 2\pi].$$

The portion of the boundary being refined is highlighted in red. Figure 3(b) is a zoomed in illustration of that region. Figure 3(c) illustrates the local refinement. Three Gaussian panels ($N_c = 48$) are replaced

N_o	N_c	$T_{\text{orig},p}$	$T_{\text{new},p}$	$T_{\text{hbs},p}$	r_p	$T_{\text{orig},s}$	$T_{\text{new},s}$	$T_{\text{hbs},s}$	r_s
9344	128	5.01e-01	5.10e-01	1.28e+00	2.50	2.08e-02	1.02e-02	7.92e-03	0.77
18688	256	1.08e+00	9.25e-01	2.18e+00	2.36	3.44e-02	2.15e-02	1.59e-02	0.74
37376	512	2.67e+00	1.30e+00	3.49e+00	2.69	5.64e-02	3.97e-02	3.00e-02	0.76
74752	1024	7.76e+00	2.31e+00	6.63e+00	2.87	1.16e-01	8.67e-02	6.40e-02	0.74
149504	2048	2.48e+01	4.06e+00	1.19e+01	2.92	2.34e-01	1.71e-01	1.61e-01	0.94

Table 3: Times for applying the solution techniques to (1) on the square with fixed nose geometry.

N_o	N_c	k_{op}	k_{kc}	k_{pk}	k_{kp}	k_{orig}	k_{new}
9344	128	87	12	45	53	272	99
18688	256	80	14	47	55	397	116
37376	512	96	14	45	55	667	114
74752	1024	117	16	46	59	1203	121
149504	2048	125	18	46	56	2237	120

Table 4: Observed numerical ranks for compressed matrices in the original and new extended system formulations for the square with fixed nose geometry.

with N_p discretization points ($N_p/16$ Gaussian panels). The number of discretization points on Γ_k remains fixed; $N_k = 6352$. The Dirichlet data is generated similarly as in Section 4.1.

Table 5 reports on the performance of all three solution techniques for this problem. The proposed solution technique is 13 to 21 times faster than building a new solver from scratch while applying the solver is less than a factor two slower than applying the HBS approximate inverse.

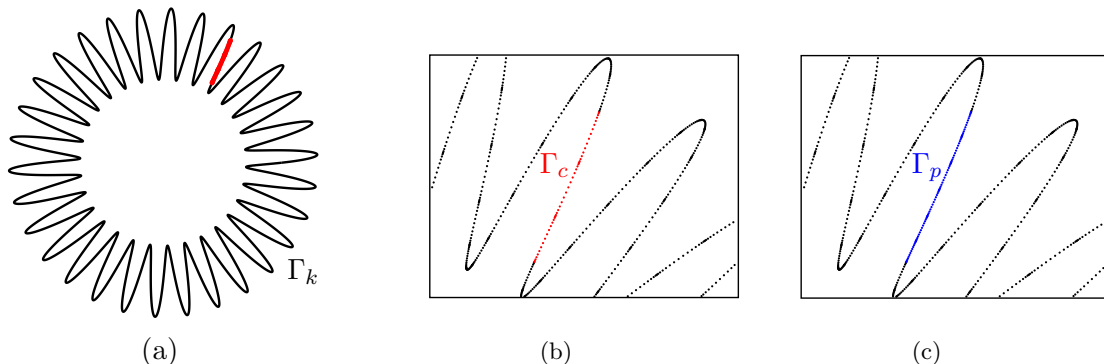


Figure 3: (a) The sunflower geometry with the portion of the boundary to be refined in red. (b) The three Gaussian panels in the boxed region from the original discretization. (c) Six Gaussian panels replacing the original three panels.

4.3 A Helmholtz problem with a locally refined discretization

Besides being faster than the solver for the original extended system, the proposed solver has the advantage that it can easily handle problems that are using specialized quadrature for weakly singular kernels. The issue that arises for the original extended system is that it would be cumbersome to evaluate the entries of the matrix \mathbf{A}_{op} corresponding to the interaction of Γ_c with Γ_p . This matrix does not arise in the new

N_p	$\frac{N_p}{N_o}$	$T_{\text{orig},p}$	$T_{\text{new},p}$	$T_{\text{hbs},p}$	r_p	$T_{\text{orig},s}$	$T_{\text{new},s}$	$T_{\text{hbs},s}$	r_s
96	0.015	6.06e-01	5.03e-01	7.52e+00	14.9	1.10e-02	1.30e-02	1.32e-02	1.02
192	0.03	6.16e-01	3.62e-01	7.77e+00	21.4	1.17e-02	1.25e-02	9.30e-03	0.74
384	0.06	6.83e-01	3.90e-01	7.72e+00	19.8	1.36e-02	1.42e-02	9.13e-03	0.64
768	0.12	7.60e-01	4.11e-01	7.78e+00	18.9	2.01e-02	1.20e-02	9.06e-03	0.76
1536	0.24	1.01e+00	6.09e-01	8.03e+00	13.2	4.72e-02	1.66e-02	1.00e-02	0.60

Table 5: Times for applying the solution techniques to (1) on the geometry in Figure 3 with local refinement.

extended system.

To illustrate the efficiency of the solver for systems that involve specialized quadrature, we consider the following exterior Dirichlet Helmholtz boundary value problem

$$\begin{aligned} -\Delta u(\mathbf{x}) + \omega^2 u &= 0 & \text{for } \mathbf{x} \in \Omega^c, \\ u(\mathbf{x}) &= g(\mathbf{x}) & \text{for } \mathbf{x} \in \Gamma \end{aligned} \quad (11)$$

with Sommerfeld radiation condition on the sunflower geometry illustrated in Figure 3 where ω denotes the wave number. The Dirichlet data g is set to be the negative of a plane wave with incident angle $\theta = -\frac{\pi}{5}$

$$g(\mathbf{x}) = -e^{i\mathbf{k} \cdot \mathbf{x}}, \text{ with } \mathbf{k} = (\omega \cos \theta, \omega \sin \theta).$$

We chose to represent the solution with the following combined field

$$u(\mathbf{x}) = \int_{\Gamma} D_{\omega}(\mathbf{x}, \mathbf{y}) \sigma(\mathbf{y}) ds(\mathbf{y}) - i\omega \int_{\Gamma} S_{\omega}(\mathbf{x}, \mathbf{y}) \sigma(\mathbf{y}) ds(\mathbf{y}), \quad (12)$$

where $\sigma(\mathbf{x})$ is the unknown boundary charge distribution, $S_{\omega} = G_{\omega}(\mathbf{x}, \mathbf{y})$ and $D_{\omega} = \partial_{\mathbf{n}(\mathbf{y})} G_{\omega}(\mathbf{x}, \mathbf{y})$ denote the single and double layer Helmholtz kernel, $\mathbf{n}(\mathbf{y})$ is the outward facing normal vector, and $G_{\omega}(\mathbf{x}, \mathbf{y}) = \frac{i}{4} H_0^{(1)}(\omega|\mathbf{x} - \mathbf{y}|)$ is the two dimensional free space Green's function for the Helmholtz equation with wave number ω and $H_0^{(1)}$ is the Hankel function of zeroth order.

The integral equation that results from enforcing the Dirichlet boundary condition is

$$\frac{1}{2} \sigma(\mathbf{x}) + \int_{\Gamma} D_{\omega}(\mathbf{x}, \mathbf{y}) \sigma(\mathbf{y}) ds(\mathbf{y}) - i\omega \int_{\Gamma} S_{\omega}(\mathbf{x}, \mathbf{y}) \sigma(\mathbf{y}) ds(\mathbf{y}) = g(\mathbf{x}). \quad (13)$$

We discretize the operator via Nyström with a composite 16-point generalized Gaussian quadrature [7]. The wave number is set to $\omega = 20$ which corresponds to the geometry being approximately 8.3 wavelengths in size. Again, we consider the local refinement problem. Table 6 reports on the performance of the proposed solution technique and building a fast direct solver from scratch. For this problem, the proposed solver is anywhere from 15 to 35 times faster than building the fast direct solver from scratch. This speed up is the result of the increased ranks associated with Helmholtz problems. Applying the proposed solver to a right-hand-side is roughly 1.5 times slower than applying the HBS solver.

5 Concluding remarks

This manuscript presented a new extended linear system for integral equation based solution techniques for boundary value problems on locally perturbed geometries. A fast direct solver based on the new extended system formulation is significantly faster than building a new direct solver from scratch for the

N_p	$\frac{N_p}{N_o}$	$T_{\text{new},p}$	$T_{\text{hbs},p}$	r_p	$T_{\text{new},s}$	$T_{\text{hbs},s}$	r_s
96	0.015	1.13e+00	3.97e+01	35.2	4.06e-02	2.86e-02	0.71
192	0.03	1.36e+00	4.08e+01	29.9	4.64e-02	2.93e-02	0.63
384	0.06	1.44e+00	4.08e+01	28.4	3.91e-02	2.54e-02	0.65
768	0.12	1.64e+00	4.17e+01	25.4	3.69e-02	2.70e-02	0.73
1536	0.24	2.64e+00	4.08e+01	15.4	4.39e-02	3.33e-02	0.76

Table 6: Times for applying the solution techniques to (11) on the geometry in Figure 3 with local refinement.

perturbed problem. For some examples, the precomputation is between 10x to 30x faster than building a direct solver from scratch. Additionally, the new solver shows consistent speed-ups for problems with a large number of points removed and can be easily applied to problems requiring the discretization of weakly singular kernels. Neither of these was true for the fast direct solver based on the original formulation given in [9].

The idea of handling local changes in geometry or discretization via the extended system formulation can be extended to three dimensional problems. However, additional work is required in processing the geometry and creating efficient techniques for building the low rank factors of the update matrix. This is future work.

References

- [1] S. Chandrasekaran and M. Gu A divide-and-conquer algorithm for the eigendecomposition of symmetric block-diagonal plus semiseparable matrices. *Numerische Mathematik*, 96(4):723-731, 2004
- [2] C. Epstein and M. O’Neil. Smoothed Corners and Scattered Waves. *SIAM Journal on Scientific Computing*, 38, 2015
- [3] A. Gillman, P. Young and P.G. Martinsson A direct solver $O(N)$ complexity for integral equations on one-dimensional domains. *Frontiers of Mathematics in China*, 7:217-247, 2012
- [4] L. Greengard, D. Gueyffier, P.G. Martinsson and V. Rokhlin Fast direct solvers for integral equations in complex three-dimensional domains. *Acta Numerica*, 18:243-275, 2009
- [5] W. Hackbusch A Sparse Matrix Arithmetic Based on H-Matrices; Part I: Introduction to H-Matrices. *Computing*, 62:89-108, 1999
- [6] K. Ho and L. Ying Hierarchical Interpolative Factorization for Elliptic Operators: Integral Equations. *Communications on Pure and Applied Mathematics*, 69, 2013
- [7] P. Kolm and V. Rokhlin Numerical quadratures for singular and hypersingular integrals. *Computers and Mathematics with Applications*, 41:327-352, 2001
- [8] Z. Sheng, P. Dewilde and S. Chandrasekaran Algorithms to solve hierarchically semi-separable systems. *Operator Theory: Advances and Applications*, 176: 255-294, 2007
- [9] Y. Zhang and A. Gillman. A fast direct solver for boundary value problems on locally perturbed geometries. *Journal of Computational Physics*, 356: 356 - 371, 2018